Available online at www.sciencedirect.com
SCIENCE DIRECT
Microelectronic Engineering 83 (2006) 1216–1220
MICROELECTRONIC ENGINEERING
www.elsevier.com/locate/mee

Micro/nanomechanical resonators for distributed mass sensing with capacitive detection

Julien Arcamone [a,*], Gemma Rius [a], Gabriel Abadal [b], Jordi Teva [b], Nuria Barniol [b], Francesc Pérez-Murano [a]

[a] Centro Nacional de Microelectrónica CNM-IMB-CSIC, Campus UAB, 08193 Bellaterra, Spain
[b] Departament d'Enginyeria Electrònica. Edifici Q, Campus UAB, 08193 Bellaterra, Spain

Available online 21 February 2006

Abstract

Micro/nanomechanical resonators have been designed and fabricated with the aim to be used as distributed mass sensors for in situ measurement of the thickness of ultra-thin layers. First, we present a comparative study of three kinds of oscillating devices (cantilever, bridge and quad beam). The quad beam design has been selected for fabrication because it combines high sensitivity and good electrical response. The complete fabrication process of the device is based on electron beam lithography, lift-off and reactive ion etching. The frequency response has been characterized by means of electrical excitation and capacitive read-out.

Keywords: Nano–micromechanical resonators; Distributed mass sensing; Capacitive detection; Monolithic integration

1. Introduction

Mass measurement based on resonating micro and nanomechanical devices has been a subject of growing interest in the last few years [1–3]. The principle of operation is based on the detection of the shift of resonance frequency when a small quantity of mass is deposited on top of the mechanical structure. In general, the smaller the resonator, the more sensitive it is because the relative change of mass is greater. Compared to quartz microbalances, micro and nanomechanical resonators offer advantages in terms of sensitivity and integration. In addition, if they are small enough, they can provide mass sensing with spatial resolution.

Silicon based micro and nanomechanical devices can be fabricated in batch using standard silicon technology process. Moreover, they can be combined with CMOS technology to fabricate monolithic integrated microsystems. This allows the assembly of arrays and matrices of resonators [4], and the development of portable systems with integrated read-out circuitry for signal processing and conditioning.

Up to now, most of the efforts have been focused on punctual single-particle mass detection [5,6], and the design of the corresponding mechanical device has been optimized for such an application. However, for distributed mass sensing (i.e., mass detection per unit area), an optimization of the device geometry is required. In this paper, we present the design and fabrication of mechanical mass sensors for measuring the thickness of ultra-thin layers. The sensor will be used in positioning as an alignment tool for nanostencil-based lithography [7]. It will detect the mass deposition rate after the atom beam flows through stencil apertures. Beam diameter is expected to be of few micrometers when impacting on the sensor surface.

As it will be shown below, by decreasing the dimensions of the mechanical resonator, sensitivity better than the state-of-the-art quartz microbalances can be achieved. Let us consider the following equation:

$$\Delta m = AS\Delta f = A\rho Rt \tag{1}$$

* Corresponding author. Tel.: +34 93 594 77 00; fax: +34 93 580 14 96.
E-mail address: julien.arcamone@cnm.es (J. Arcamone).

0167-9317/$ - see front matter © 2006 Elsevier B.V. All rights reserved.
doi:10.1016/j.mee.2006.01.177

hence,

$$\Delta f = \frac{\rho R t}{S} \tag{2}$$

where Δm is the mass of the on-top deposited layer, S the distributed mass sensitivity (g cm^{-2} Hz^{-1}), Δf the resulting frequency shift, A the resonator area, ρ the density of the deposited material, R the evaporation rate (nm/s) and t the evaporation time.

Then, for the purpose of the final application (in situ ultra-thin layer detection, i.e., in an evaporation chamber under vacuum conditions), we aim to measure a frequency shift corresponding to a 1 s shutter aperture time for a typical deposition rate of 0.3 nm/s for gold and aluminum. From initial tests performed in air (see Section 4), we assume 0.5 kHz as the minimum detectable frequency shift. In Table 1, the frequency shift as a function of the sensitivity for the two materials of interest is depicted.

We conclude that the appropriate range for the mass sensitivity is 10^{-10}–10^{-11} g cm^{-2} Hz^{-1}, i.e., more sensitive than state of the art quartz microbalances.

For the read-out of the resonator oscillation, optical characterization offers very high resolution under various configurations (through interferometer methods [8] or with atomic force microscopy based set-ups) but its implementation is not adequate in the present application because the sensor will be covered by the stencil membrane. Consequently, the read-out has to be based on electrical methods; in addition to its easy implementation, it will allow the monolithic integration of the sensor with CMOS circuits [9].

2. Modeling

We compare, in terms of mass sensitivity and electrical response, three types of silicon mechanical resonators operating in the fundamental vertical flexural mode: cantilever (Fig. 1a), bridge (Fig. 1b) (common structures used for mass sensing [5,10]) and quad beam resonator (Fig. 1c).

2.1. Comparative study in terms of distributed mass sensitivity (S)

Let us consider a general law for the resonance frequency,

$$f_i = \frac{1}{2\pi}\sqrt{\frac{k_i}{m_{\text{eff}}}} \tag{3}$$

Table 1
Frequency shift associated to a given distributed mass sensitivity for a 1 s deposition at a rate of 0.3 nm/s for gold and aluminum

Sensitivity (g cm^{-2} Hz^{-1})	1E−09	1E−10	1E−11
Gold ($\rho = 19.3$ g cm^{-3})	$\Delta f = 0.58$ kHz	$\Delta f = 5.8$ kHz	$\Delta f = 58$ kHz
Aluminum ($\rho = 2.7$ g m^{-3})	$\Delta f = 0.08$ kHz	$\Delta f = 0.8$ kHz	$\Delta f = 8$ kHz

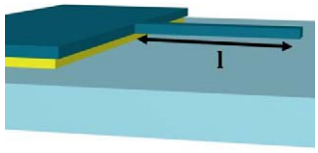

Fig. 1a. Cantilever oscillator with length l as characteristic dimension.

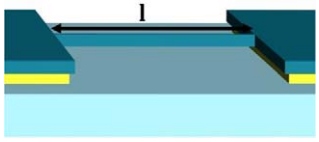

Fig. 1b. Bridge oscillator with length l as characteristic dimension.

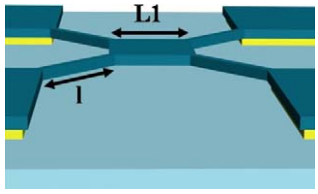

Fig. 1c. Quad beam oscillator with paddle width $L1$ as characteristic dimension, and l as beam length.

where f_i is the resonance frequency of a given mode i. The spring constant, k_i, and the effective mass, m_{eff}, both depend on the oscillation mode and on the force loading distribution and point of application. In case, k_i and m_{eff} correspond to a uniform mass (i.e., force) loading in the first vertical flexural mode ($f_i = f_o$). The mass sensitivity can be evaluated from:

$$\frac{\partial m}{\partial f} \approx \frac{1}{2\pi^2}\frac{k}{f_o^3} = 2\frac{m_{\text{eff}}}{f_o} \quad (\text{g Hz}^{-1}) \tag{4}$$

$$\text{and} \quad S = \frac{1}{A}\frac{\partial m}{\partial f} \quad (\text{g cm}^{-2}\ \text{Hz}^{-1}) \tag{5}$$

where A is the resonating area exposed to mass loading. Applying Eqs. (3)–(5) to the three structures of Fig. 1, we find that for any kind of structure vibrating in flexion, the following quantity:

$$\frac{f_o S}{h} = C_s$$

only depends on the material properties and the specific mode. Indeed C_s can also be written as

$$C_s = 2\rho\alpha_{\text{eff}} \quad \text{and} \quad \alpha_{\text{eff}} = \frac{m_{\text{eff}}}{m}$$

with m the resonator mass and h its thickness. Therefore, for a given thickness, the higher the resonance frequency, the better is the sensitivity.

Table 2 shows the values of the characteristic parameters for the three types of devices. Based on them, we have plotted, in Fig. 2, S (distributed mass sensitivity) as a function of l and $L1$ (characteristic length of each device

Table 2
Basic equations used to compare quantitatively three kinds of resonators in their vertical flexural mode for a mass electrical sensing purpose, where w is the beam width, h the beam thickness,l the beam length, E the Young's modulus, ρ the density of structure material, $L1$ the paddle width

	Cantilever	Bridge	Quad beam [a]
k, spring constant for uniform mass loading	$\frac{2}{3}\frac{E\cdot h^3\cdot w}{l^3}$	$32\frac{E\cdot h^3\cdot w}{l^3}$	$1.5\frac{E\cdot h^3\cdot w}{l^3}$
$\alpha_{\text{eff}} = m_{\text{eff}}/m_{\text{resonator}}$	0.65	0.75	1
f_o, fundamental resonance frequency	$\frac{1.015}{2\pi}\sqrt{\frac{E}{\rho}}\frac{h}{l^2}$	$\frac{6.5}{2\pi}\sqrt{\frac{E}{\rho}}\frac{h}{l^2}$	$\frac{1.2}{2\pi}\sqrt{\frac{E}{\rho}}\frac{h\cdot w^{0.5}}{l\cdot L1^{1.5}}$
$C_s = f_o\cdot S/h$	3000	3500	4600
S (g cm^{-2} Hz^{-1})	$0.225\cdot l^2$	$0.041\cdot l^2$	$0.291\frac{L1\cdot l^{1.5}}{w^{0.5}}$
FM with $\left\{\gamma = \frac{Q\cdot\varepsilon o^2\cdot V_{\text{dc}}^2}{(C_{\text{ox}}+C_{\text{w}})\cdot d^4 E\cdot h^3}\right\}$	$\frac{3}{2}\gamma\cdot l^5\cdot w$	$\frac{1}{32}\gamma\cdot l^5\cdot w$	$\frac{2}{3}\gamma\cdot\frac{L1^4\cdot l^3}{w}$

[a] In the quad beam column indicates that these formulas are the result of an experimental fit that corrects a discrepancy with theoretical formulas. It is due to the under-etching of resonators anchors that occur during the last fabrication step, the SiO_2 etching to release free standing structures.

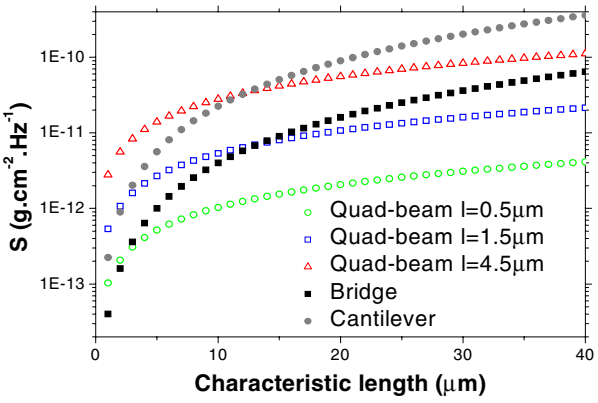

Fig. 2. Distributed mass sensitivity for three kinds of resonators for $w = 1$ μm, $h = 300$ nm as a function of the characteristic dimension.

defined as the largest dimension of the sensitive area) for constant thickness ($h = 300$ nm) and width ($w = 1$ μm).

It can be observed that the cantilever is less sensitive than the other two types of mechanical resonators. Comparing bridge and quad beam resonators, their relative sensitivity depends on the value of the characteristic length.

2.2. Comparative study in terms of electrical response

As it has been mentioned previously, the final goal is the monolithic integration of the mechanical resonators with CMOS readout circuitry. This means that both actuation and detection have to be electrical. For the three types of devices, actuation is performed by applying a voltage (AC + DC) between resonator and substrate. For evaluating the electrical response, and taking into account parasitic capacitances, we have built up a figure of merit (FM) thus defined:

$$\text{FM}\ (\%) = 100\frac{i_{\text{NEMS}}}{i_{C_{\text{ox}}} + i_{C_{\text{w}}}} \tag{6}$$

calculated at the resonance frequency. $i_{C\text{ox}}$ is the capacitive current due to the physical capacitor $Si/SiO_2/Si$ between resonators anchors, lines and pads, and the substrate; $i_{C\text{w}}$ is due to the static plate/air/substrate capacitor (modeled as parallel finite plates with constant gap d). i_{NEMS} is the capacitive current produced at resonance by mechanical motion of the resonator. Its value is calculated via a RLC model [11–13] as follows:

$$i_{\text{NEMS}} = \frac{V_{\text{ac}}}{R_{\text{m}}} \quad \text{with } R_{\text{m}} = \frac{\sqrt{km}}{Q\eta^2} \tag{7}$$

$$\text{with} \quad \eta = \frac{\varepsilon_0 A V_{\text{dc}}}{d^2} \tag{8}$$

where Q is the resonator quality factor, ε_0 the dielectric constant, A the resonator area, V_{dc} the applied DC voltage, and d the gap.

Inserting (8) into (7) and computing it with (6) leads to a global equation:

$$\text{FM}\ (\%) = 100\frac{Q\varepsilon_0^2 A^2 V_{\text{dc}}^2}{d^4(C_{\text{ox}} + C_{\text{w}})}\cdot\frac{1}{k} \tag{9}$$

For device specific FM calculation, values in Table 2 are used. We have plotted FM, in Fig. 3, as a function of l and $L1$ for constant thickness ($h = 300$ nm), width ($w = 1$ μm) and gap ($d = 1$ μm).

Globally, the quad beam oscillator offers better performance to reach the FM = 10% threshold that can be considered as the minimum for effective detection. Consequently, in the range 10^{-10}–10^{-11} g cm^{-2} Hz^{-1} of mass sensitivity, the quad beam offers the best compromise between electrical response and measurement accuracy.

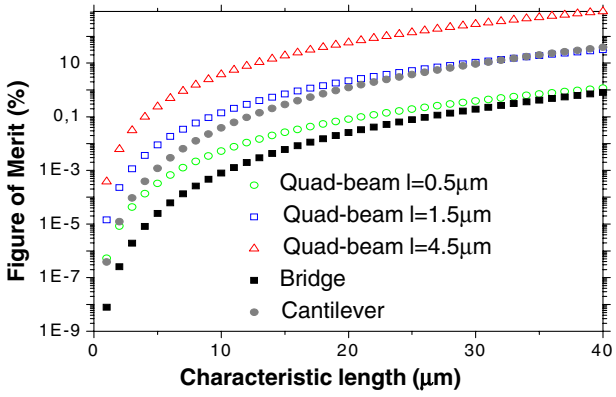

Fig. 3. Electrical figure of merit (FM) for three kinds of resonators for $w = 1$ μm, $h = 300$ nm as a function of characteristic dimension.

3. Fabrication process

Resonating devices have been fabricated using a technological process based on standard silicon surface micromachining of silicon-on-insulator (SOI) wafers. The thickness of the SOI layer is 1.5 μm, the thickness one of the SiO_2 is 1 μm. First, the top silicon layer is n-doped by diffusion of phosphor at high temperature (surface doping: $N_d \approx 10^{18}$ at cm^{-3}). Then doping impurities are thermally activated under O_2 and N_2 atmosphere.

In order to decrease physical parasitic capacitances (see Section 2.2), pads and anchors area has been minimized and they are only made of doped silicon (no metal contact is required). Therefore, for the whole process, a single lithography step is necessary. After doping, samples are coated with 115 nm of poly(methylmethacrylate) resist and patterned by electron beam lithography with a 10 kV electron beam. This technique allows obtaining submicron features and provides much flexibility for prototyping. After resist exposure and development, a 24 nm thick aluminum layer is evaporated on top of the samples. This is followed by a lift-off process, based on heated acetone under ultrasound vibration, optimized for nanometer scale features. Aluminum is used as mask for the subsequent reactive ion etching (RIE) of silicon because of its excellent selectivity with respect to it even for very thin layers (24 nm) what makes the lift-off easier. For an etch speed of about 1 μm per minute, the RIE recipe (performed on Alcatel A601E) is based on the BOSCH plasma etching process at room temperature: C_4F_8 and SF_6 gases are alternatively injected into the reaction chamber, respectively, for vertical flanks passivation and silicon etching. Then, small features are released by selective wet under-etching of SiO_2 in a buffered HF solution. Fig. 4 shows scanning electron micrographs of mechanical resonators at the end of the process. Fig. 4b reveals that the mechanical structure is successfully released from the substrate.

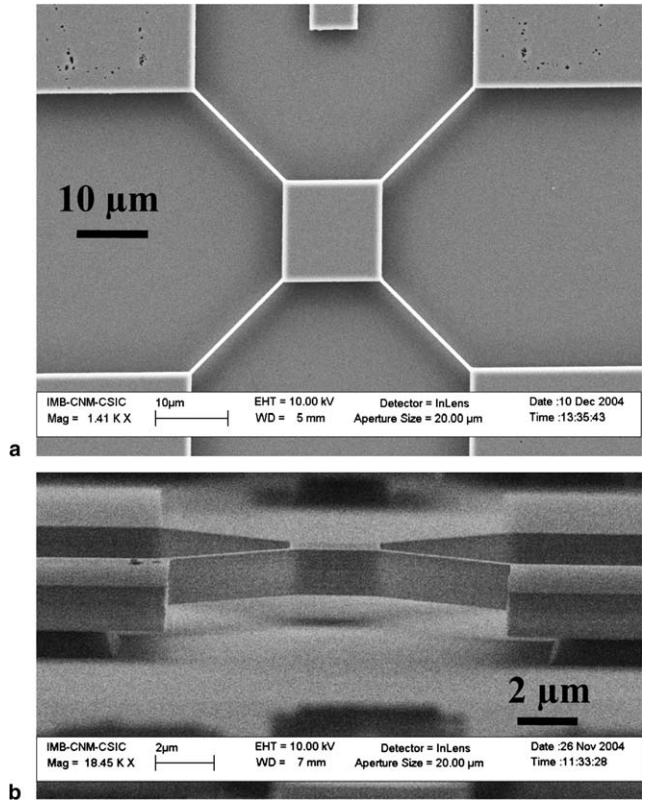

Fig. 4. (a, b).Scanning electron microscopy (SEM) pictures of a fabricated Si micro nanoresonator made on SOI wafer: above in top-view, below in tilted view.

4. Resonance detection by electrical measurements

First prototypes of quad beam resonators were measured in air. An AC voltage (<10 V) plus DC voltage (50–100 V) is applied to the substrate. The resonator layer is grounded via a contact probe connected to a network analyzer that allows measuring the total capacitive current (sum of parasitic, static and resonance contributions). The frequency response is affected by the applied DC voltage [14]. Indeed, assuming that the electrostatic force F_e, acting on the central paddle, is equal to that for a parallel plate capacitor:

$$F_e = -\frac{\varepsilon_0 \cdot L_1^2}{2 \cdot (d-z)^2} V_{dc}^2 \tag{10}$$

and combining (10) with Newton's law and Eq. (3), it gives:

$$f(V) = f_0 \cdot \left(1 - \frac{\varepsilon_0 l^4}{d^3 E h^2 w} V_{dc}^2\right) \quad \text{for } V_{dc} \gg V_{ac} \text{ and } d \gg z \tag{11}$$

With a quad beam resonator of the following dimensions: $L1 = 14$ μm, $l = 18$ μm, $w = 0.55$ μm, $h = 1.5$ μm (whose theoretical FM is ≈14%), we have obtained the curves shown in Figs. 5a and 5b.

The amplitude shows one maximum and one minimum corresponding to resonance and anti-resonance respectively. The anti-resonance is related to parasitic capacitances. Future integration with CMOS is expected to

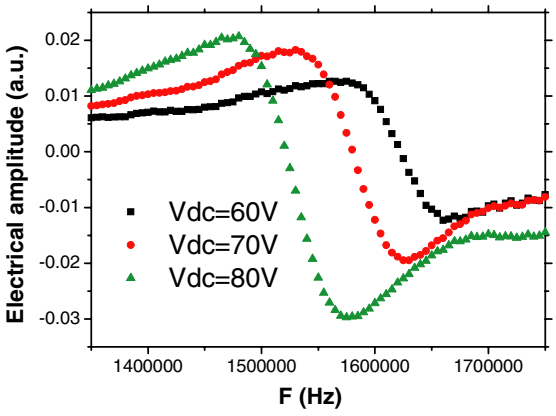

Fig. 5a. Resonance curves of the amplitude signal for several applied DC voltages.

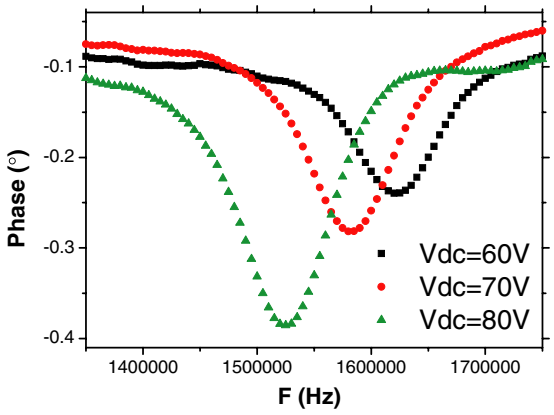

Fig. 5b. Resonance curves of the phase signal for several applied DC voltages.

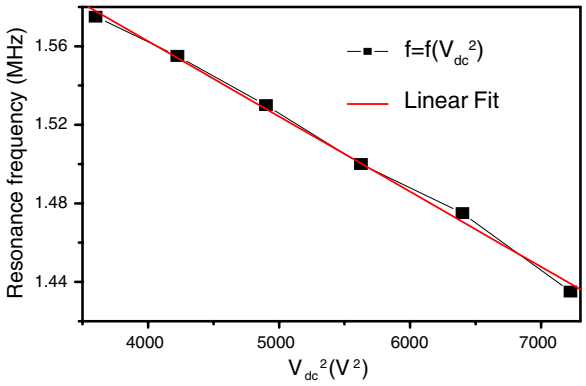

Fig. 6. Experimental curve and subsequent linear fit of the voltage dependant resonance frequency as a function of the squared applied voltage.

reduce them. Then, representing the maximum of the amplitude as a function of V_{dc}^2 (cf. Eq. (11)), we can obtain f_0:

As it can be observed in Fig. 6, the linear fit is good and the value of $f_0(V_{DC} = 0)$ is around 1.72 MHz. This is in good agreement with analytical mechanical calculations, based on Rayleigh-Ritz quotient [15], that we have been making in order to take into account the behavior of released anchor edges due to under-etching of SiO_2 happening at the end of the fabrication process.

From the experimental characterization, a theoretical sensitivity of 4×10^{-10} g cm^{-2} Hz^{-1} is deduced. By optimizing the dimensions of the mechanical device, the range 10^{-10}–10^{-11} of sensitivity can be easily reached, for example with a quad beam resonator of the following dimensions: $L1 = 13$ μm, $l = 5$ μm, $w = 0.55$ μm, $h = 0.3$ μm (with a theoretical FM around 20% in air).

5. Conclusion and perspectives

We have demonstrated the fabrication, actuation and detection of a specific micro/nanomechanical resonating structure based on a quad beam configuration. It has been chosen among more classical geometries (cantilever or bridge), because it responds to the conjugated requirements of a good sensitivity for distributed mass sensing and because it provides a better signal for electrical read-out. The first prototypes have been successfully tested. Currently, we are fabricating similar devices integrated with CMOS circuits that will allow performing 'in situ' experiments of distributed mass sensing, providing an enhanced resonance signal.

Acknowledgements

This work has been partially funded by the EU IP NaPa project (Contract No. NMP4-CT-2003-500120) and by the project TIC2003-07237-C01 from the Spanish MCYT.

References

[1] K.L. Ekinci, M.L. Roukes, Rev. Sci. Inst. 76 (2005).
[2] R. Berger et al., Microelectron. Eng. 35 (1997) 373.
[3] A. Boisen, J. Thaysen, H. Jensenius, O. Hansen, Ultramicroscopy 82 (2000) 11.
[4] M. Villarroya et al., in: Proceedings of XIX Eurosensors, Barcelona, 11–14 September, 2005.
[5] L.B. Sharos et al., Appl. Phys. Lett. 84 (23) (2004) 4638.
[6] B. Ilic, H.G. Craighead, et al., J. Appl. Phys. 95 (2004) 3694.
[7] M.A.F. van den Boogaart et al., J. Vac. Sci. Technol. B 22 (6) (2004) 3174.
[8] D.W. Carr, H.G. Craighead, et al., J. Vac. Sci. Technol. B 15 (6) (1997) 2760;
D.W. Carr, H.G. Craighead, et al., J. Vac. Sci. Technol. B 16 (6) (1998) 3821.
[9] O. Brand, G.K. Fedder, et al.CMOS-MEMS, vol. 2, Wiley-VCH, Weinheim, 2005.
[10] K.L. Ekinci, X.M.H. Huang, M.L. Roukes, Appl. Phys. Lett. 84 (22) (2004) 4469.
[11] G. Abadal et al., Nanotechnology 12 (2001) 100.
[12] C.T.-C. Nguyen et al., J. Sol.-St. Circ. 34 (4) (1999) 440.
[13] T. Mattila et al., Sensor. Actuator. A 101 (2002) 1.
[14] Z.J. Davis et al., J. Vac. Sci. Technol. B 18 (2) (2000) 612.
[15] M.-H. Bao, MicromechanicalTransducers, vol. 8, Elsevier, Amsterdam, 2000.